Materials Research Proceedings 31 (2023) 227-239 https://doi.org/10.21741/9781644902592-24

Influence of canard geometrical configuration on the radar cross section

Gauri Patki[1], Attada Phanendra Kumar[2], Dineshkumar Harursampath[2]

[1]Department of Aerospace Engineering, IIT Kharagpur, Kharagpur-721302, India

[2]Department of Aerospace Engineering, IISc Bengaluru, Karnataka, India

Keywords: Radar Cross Section, Canard Configuration, Physical Optics, Monostatic RCS, Far Field Approximation

Abstract. The Radar Cross Section (RCS) of fighter jet hold a lot of importance in determining its air superiority. Electromagnetic simulations can be performed by employing numerical methods such as MoM, ray tracing methods or Physical Optics. Configuration of the wing is an important factor in determining the overall RCS of the aircraft. The current study explores the RCS of canard as placed in Chengdu J-20. The parameters are varied, the models are created and the simulations are conducted for monostatic RCS using far field approximation over a continuous frequency range using Physical Optics in FEKO simulator. The trends in results are analyzed and promising configurations are identified.

Introduction

Stealth technology, or Low Observable technology as it is alternatively called, is a combination of military tactics and active and passive countermeasures that aim at reducing a fighter aircraft's visibility on radar, infrared, sonar or any other methods of detection [1]. Complete invisibility to the radar through stealth technology is an ideal situation. But the development and progress in the field has rendered 5th and higher generation aircrafts much less visible to the radar as compared to the older generations. Stealth technology mainly involves reduction in electromagnetic reflections and infrared footprints by reducing thermal emission from thrusts, reduction in aircraft's radar cross section and visual camouflage by blending the aircraft with the background sky. Development of specific shapes such as large surfaces, avoiding sharp curves and right angles helps in improving the stealth abilities. A combination series of curved surfaces having complex radius or several small, carefully oriented flat planes may combine to generate an exterior shape. Vertical surfaces are avoided as they significantly enhance the radar cross section. Radiation absorbent material (RAM) absorbs the EM radiation sent towards the target by the source radar or sonar. Metals and conductors have a higher reflectivity than non-conductors, so the latter is generally used as an RAM. Some examples are iron ball paint absorber in which microscopic spheres coated in carbonyl iron are suspended in the paint. They convert radiation into heat and dissipate it. Carbon nanotube is an excellent RAM but coating the entire surface with it is not feasible. The use of RAM in the early aircrafts made them heavy and not strong even for structural use at high altitudes. Hence, the focus remains mainly on reducing the RCS of the aircraft.

Research comprising of simulation and analysis of different generation of aircrafts such as Valkyrie and F-16 for RCS calculation have been conducted. It was seen in these studies that the Valkyrie aircraft had a large RCS despite being ahead of performance in time. On the other hand, the F-16 aircraft had a very low RCS and has survived a long time being harder to spot making it a prolific fighter. Further in the study, tailless configuration was considered as a candidate for stealth analysis. This configuration gave almost zero RCS except for a few angles in roll, pitch and yaw planes [2].

While there has been a certain progress in designing the shape of the aircraft, the methods for RCS calculation have also been improved. In order to devise better methods for RCS estimation,

Materials Research Proceedings 31 (2023) 227-239 https://doi.org/10.21741/9781644902592-24

calculation abilities based of numerical schemes such as MoM, MLFMM and HOBF have also been explored and researched [3]. Studies comparing models for dynamic RCS calculation have shown that Gaussian Mixture Density Model (GMDM) gives better approximation compared to Chi-Square and Log-normal distribution [4]. The sparse-matrix method (SMM) algorithm generates matrices that take shorter running time than those generated by Method of Moments (MOM) [5]. RCS modelling validation has also been done by experimenting on a full- scale aircraft, the data being obtained from the experimentation, processed, analyzed and compared with the results from simulations for validation [6].

Different aircraft configurations arose in the past decades as a result of efforts towards obtaining least radar visibility. While most fighter jets adopt the conventional layout, the Chinese 5th generation fighter jet, Chengdu J-20 deviates with its duck layout, i.e., the presence of canards on the frontal part of the aircraft. It has been observed that addition of canards gives the aircraft an aerodynamic advantage [7]. However, it is also equivalent to adding a scattering component in the front as the movable gap between the fuselage and the canard is directly exposed in the front. The deflection of canards thus increases the RCS of the nose of the aircraft significantly.

The previous studies conducted in the field of RCS explore the measurement and calculation of RCS via different method and application of various algorithm. There have been comparisons between conventional and duck layout to understand how differing from conventionality affects the stealth and if the effect is drastic or not [7]. This work attempts to understand how change in certain parameter at a time affect the RCS of the aircraft considering every other aspect to remain the same. Forming the duck layout, a canard poses as a means to bring significant change in the RCS of the aircraft on the whole. Hence, it is required to find geometrical parameters such that this effect is not drastic.

Objective

The current study explores the RCS of canard having original parameters as that of J-20 and then proceeds to calculate the RCS of canards modelled by varying parameters. The CAD models are created in SOLIDWORKS and simulated using Altair FEKO simulation software. The graphs are then obtained. The focus of the study is upon the structural aspects of the canard as the only target under observation without considering the attachment to the fuselage. How the RCS is affected by variation in the geometrical parameters of the canard is observed.

Radar Cross Section (RCS) For Different Cross-Section Profiles

Radar cross section is basically the cross section of a perfectly reflecting sphere that will reflect the same strength of signal as the aircraft in question. RCS describes the amount of scattered power from the target towards the Radar. It is the measure of the ratio of backscatter power per steradian (unit solid angle) in the direction of the radar to power density that is intercepted by the target [8]. Higher the RCS, more detectable is the aircraft.

The basic equation for RCS calculation is given as:

$$\sigma = \lim_{R \to \infty} 4\pi R^2 \frac{E_S^2}{E_0^2}$$

where,

σ = radar cross section

R = range of the target

E_S = amount of reflected power from the target

E_0 = power density of wave incident on the target

RCS is measured in dBsm (decibel square meter). The unit conversion from dBsm to m2 is given as:

$$\text{dBsm} = 10 \times \log_{10}\left(\frac{RCS}{1\ m^2}\right)$$

Materials Research Proceedings 31 (2023) 227-239 https://doi.org/10.21741/9781644902592-24

Mathematical formulations for the RCS of some basic shapes such as sphere, cylinder, ellipsoid and triangular plate have been reported [4].

1. **Sphere**

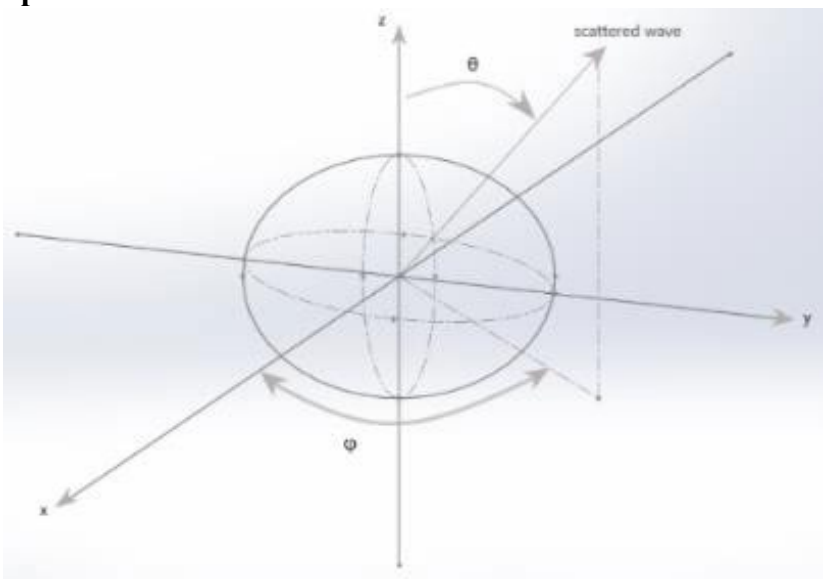

$\frac{\sigma}{\pi r^2} = \frac{1}{kr}\sum_{n=1}^{\infty}(-1)^n\,(2n+1)[\left(\frac{kr\,j_n(kr) - n\,j_n(kr)}{krH_n - 1(kr) - nH_n^1(kr)}\right) - (\frac{j_n(kr)}{H_n^1(kr)})]$

Where,

k = 2π/λ, λ is the wavelength

j_n= spherical Bessel of the first kind of order n

H_n^1= Hankel function of order n and is given by

H_n^1(kr) = j_n(kr) +jy_n(kr)

y_n= Spherical Bessel function of the second kind of order n

2. **Cylinder**

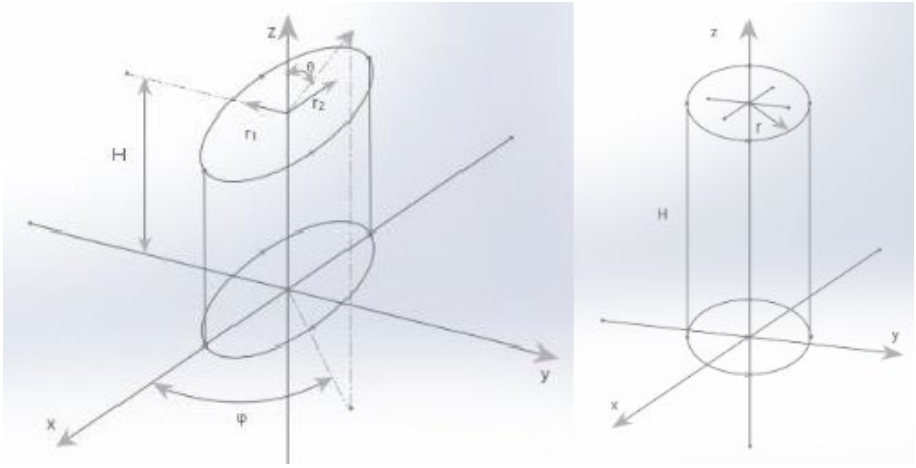

$$\sigma_{\theta n} = \frac{2\pi H^2 r_1^2 r_2^2}{\lambda(r_1^2(cos\varphi)^2 + r_2^2(sin\varphi)^2)^{1.5}}$$

$$\sigma = \frac{\lambda r_1^2 r_2^2}{8\pi(cos\theta)^2(r_1^2(cos\varphi)^2 + r_2^2(sin\varphi)^2)}$$

gives RCS for an incident wave other than normal.

Materials Research Proceedings 31 (2023) 227-239 https://doi.org/10.21741/9781644902592-24

The equations can be further reduced to obtain mathematical formulation for circular cylinder as

$\sigma_{\theta n} = \frac{2\pi L^2 r}{\lambda}$

$\sigma = \frac{\lambda r sin\theta}{8\pi(cos\theta)^2}$

where,

H = height of the cylinder

R = radius of the cylinder

3. Ellipsoid

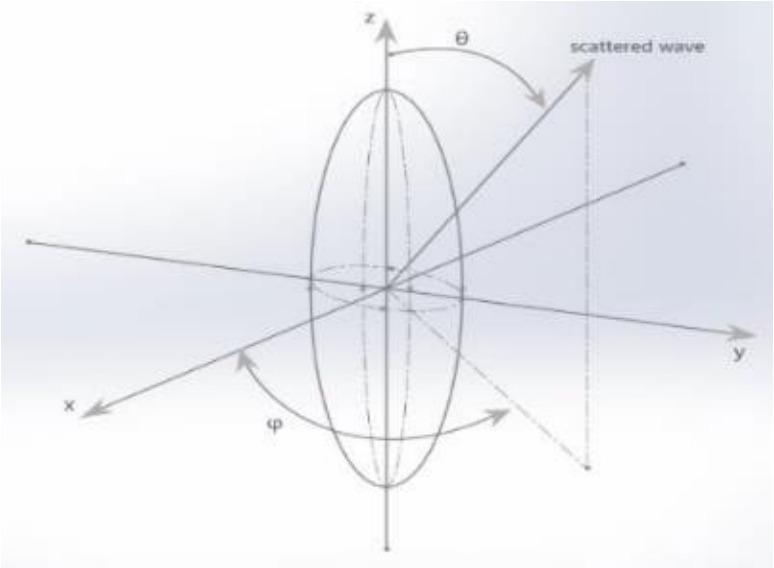

$\sigma = \frac{\pi a^2 b^2 c^2}{(a^2(sin\theta)^2(cos\varphi)^2 + b^2(sin\theta)^2(sin\varphi)^2 + c^2(cos\theta)^2)^2}$

$\sigma = \frac{\pi b^4 c^2}{(a^2(sin\theta)^2 + c^2(cos\theta)^2)^2}$, when a = b as ellipsoid becomes roll symmetric and RCS is independent of φ.

When a = b = c, σ = πc2 which is backscattered RCS of sphere.

where,

a = ellipsoid a radius

b = ellipsoid b radius

c = ellipsoid c radius

φ = roll angle

θ = angle between z axis and direction to receiving radar

Materials Research Proceedings 31 (2023) 227-239 https://doi.org/10.21741/9781644902592-24

4. **Triangular plate**

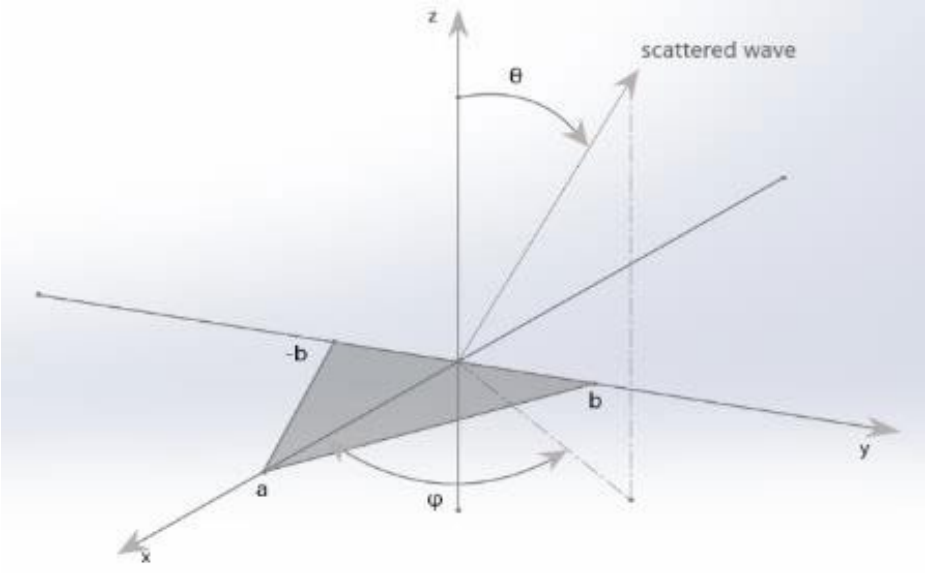

$\sigma = \frac{4\pi\lambda^2}{\lambda^2} cos\theta\sigma_0$

$\sigma_0 = \frac{\sigma_{01}+[(sin\alpha)^2-(sin^{\beta}/_2)^2]^2}{(\alpha^2-(^{\beta}/_2)^2)^2}$

$\sigma_{01} = 0.25(sin\varphi)^2(\frac{2a}{b}cos\varphi sin\beta - sin\varphi sin2\alpha)^2$

α = k a sinθ cosφ, β = k a sinθ sinφ

for φ = 0,

$\sigma = \frac{4\pi A^2}{\lambda^2}(cos\theta)^2[\frac{(sin\alpha)^4}{\alpha^4} + \frac{(sin2\alpha-2\alpha)^4}{4\alpha^4}]$

$A = \frac{ab}{2}$

For $\varphi = \frac{\pi}{2}$,

$\sigma = \frac{4\pi A^2}{\lambda^2}(cos\theta)^2[\frac{(sin\beta/2)^4}{(\beta/2)^4}]$

Methods of Computation and RCS Calculation

Computer simulations use numerical methods for the RCS prediction for arbitrary dimensional target such as modelled aircrafts. Some of the popular methods are:

1. **Method of Moments (MoM)**

   The most common yet rigorous, full-wave numerical technique to solve open boundary electromagnetic problems is Method of Moments. It solves the integral form of Maxwell's equations to predict the RCS, so, it must satisfy the said equations and relevant boundary conditions. MoM takes the currents and the fields on surface of the structure as unknowns. The structure is immersed in free space, the background medium of which is modelled using free-space Green's function [5].

   The technique is highly accurate but produces large matrices by reducing the operator equations into a system of linear equations.

2. **Ray Tracing Methods**

   Ray tracing methods consist of a collection of techniques that can be used individually or in conjunction with each other to analyse electrically large and arbitrarily shaped targets. Two most commonly used methods are Geometrical Optics (GO) and Geometrical Theory

of Diffraction (GTD). Geometrical Optics assumes that the photons or rays are reflected at the complement of the angle between the incident ray and the surface normal [6]. Thus the monostatic RCS arises only from the rays normal to the specular components such as edges, vertices and dihedrals.

Other ray tracing methods include Uniform Theory of Diffraction (UTD) and Physical Theory of Diffraction (PTD). These too analyse electrically large targets taking into account diffracted rays.

3. **Finite Difference Method**

   Finite Difference Methods discretize the target and apply the approximated differential operators in either time or frequency domain to the said discretized target [7]. The time domain involves stepping the solution in time throughout the grid on the surface. The Fourier transformation of the time domain gives the data in the frequency domain.

   Finite difference methods provide rigorous solution. However, gird refinement for the required level of accuracy makes it computationally expensive as the execution time increases.

4. **Physical Optics (PO)**

   Physical Optics is a method of estimation of electromagnetic scattering using induced currents assuming that the surface is perfectly conducting. An incident source illuminates the scatterer surface and induced electric currents from tangential magnetic fields are considered. These currents reradiate to produce the scattered field [13]. Physical Optics approximation assumes that the radiation from the illuminated part is directly proportional to the incident magnetic field intensity while that from the rest is zero [14].

   The simulations here solve the model using Physical Optics- Always illuminated solver in Altair FEKO software. This assumes that all the triangles on which PO approximation is made are illuminated [15].

Results and Discussion

The canard models were first created using SOLIDWORKS and then imported in CADFEKO. The incident plane wave was set to loop over multiple directions with $\theta = 90^\circ$ and φ between 0° and 180° with an increment of 30°. The frequency was set to be a continuous range between 1.7 GHz and 5.6 GHz [7]. Fields were calculated in the direction of plane wave incidence. Monostatic RCS is calculated using far-field approximation.

The parameters considered while modelling the canard were wing span, wing chord at root, wing chord at tip, airfoil shape and angle of incidence. Additionally, canard lift coefficient and angle of attack affect the utility of canards on an aircraft. We performed simulations over 24 models varying wing span and wing chords at the root and tip.

The tip of the root chord was placed at the origin with the root airfoil in XZ plane. The span is along the Y- axis, positive z direction id downwards positive x axis from leading edge to the trailing edge of the root airfoil.

Different geometrical specifications of canard

1. Wing chord at root and tip of the canard are approximated by scaling the dimensions of the main wing from the available information.
2. Angle of incidence of the canard in J-20 can be varied. It is taken to be 0 in all cases here.
3. Information on the type of wing airfoil of J-20 is unknown/ classified. NACA airfoils of required chord lengths, 100% thickness, 5° pitch are used to create the SOLIDWORKS models.
4. The aspect ratio (AR) varies with the models as the parameters keep changing.

Materials Research Proceedings 31 (2023) 227-239 https://doi.org/10.21741/9781644902592-24

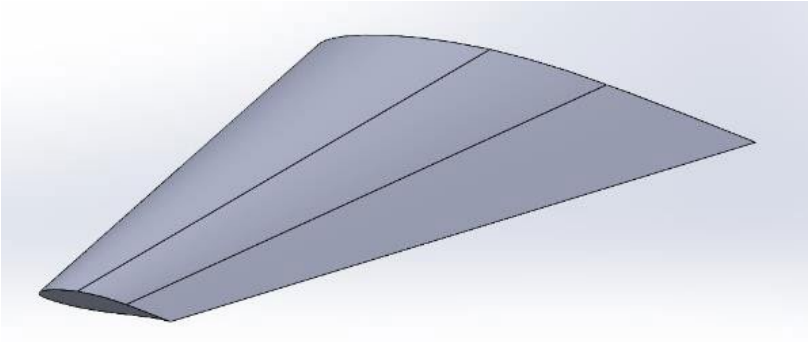

Fig 1. Canard model in SOLIDWORKS Original Canard Parameters from J20:

Wing span = 7.62m (Single canard measures 3.81m)
Wing chord (root) = 2.286 m
Wing chord (tip) = 0.6858 m
Wing aspect ratio = 2.3
Wing airfoil – unknown
Angle of Incidence – variable
(The dimensions specified are approximately scaled using the available information.)

First order GO approximations were used to obtain theoretical values of the RCS. At φ = 0˚ for 1.7 GHz frequency, considering the effective edge length to be 4.1324 m, the RCS comes out to be

$\sigma = \frac{L_{eff}^2}{\pi}$ [11]

σ = 7.35255 dBsm

The result from simulation for the same specified condition is σ = 7.95864 dBsm. While the result from the theoretical calculation was not accurate, it was still close enough. The simulation used Physical Optics coupled with other numerical techniques to increase the accuracy of the results. This might be the reason for discrepancy.

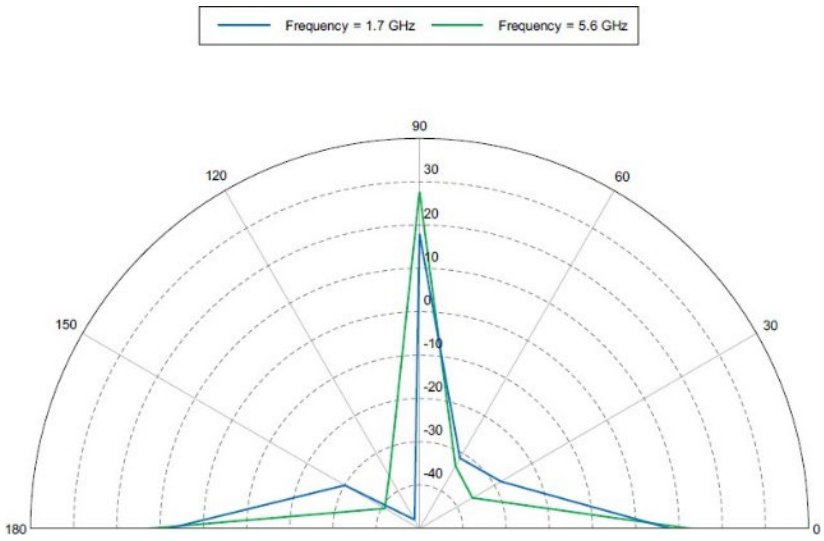

Fig 2. Polar graph for original canard

Variable Chord at Tip

Keeping all other parameters constant, 8 models were created with varying values of chord at the tip. They were simulated and the RCS was compared with that of the original canard.

Materials Research Proceedings 31 (2023) 227-239 https://doi.org/10.21741/9781644902592-24

The parameters used are given below:

Table 1. Parameters of canards with variable chord at tip

	Wing Span (one wing)	**Wing Chord (root)**	**Wing Chord (tip)**	**Aspect Ratio**
C1	3.81	2.286	0.65	**2.59**
C2	3.81	2.286	0.6	**2.64**
C3	3.81	2.286	0.55	**2.68**
C4	3.81	2.286	0.5	**2.73**
C5	3.81	2.286	0.7	**2.55**
C6	3.81	2.286	0.75	**2.50**
C7	3.81	2.286	0.8	**2.46**
C8	**3.81**	**2.286**	**0.85**	**2.42**

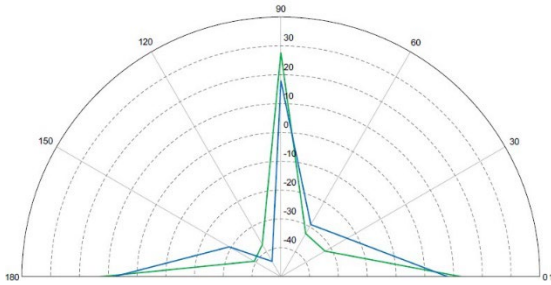

Fig 3. Polar graph for C1

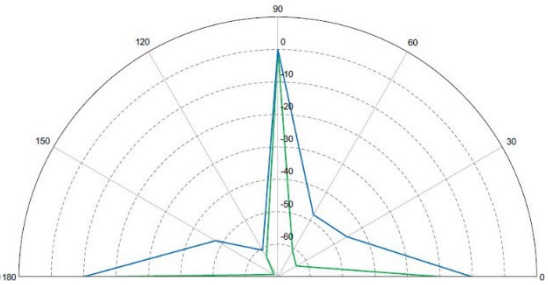

Fig 4. Polar graph for C2

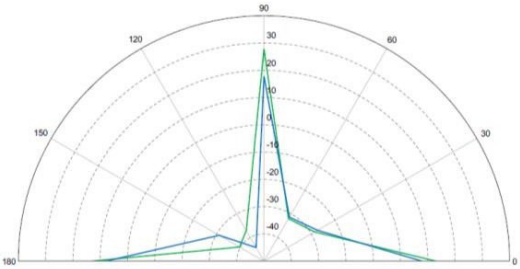

Fig 5. Polar graph for C3

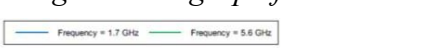

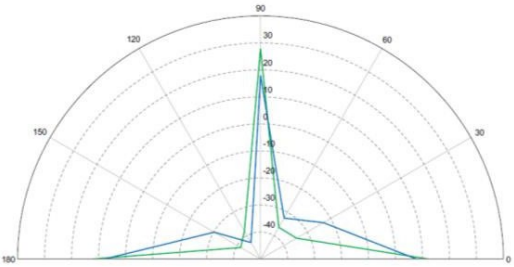

Fig 6. Polar graph for C4

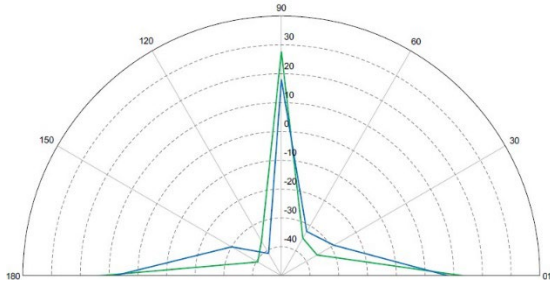

Fig 7. Polar graph for C5

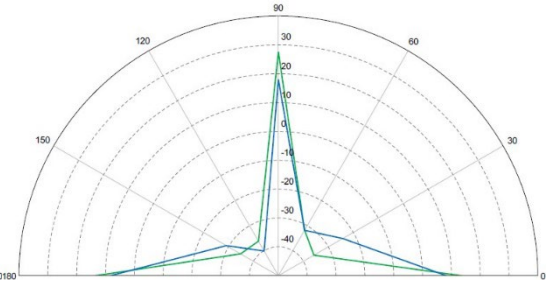

Fig 8. Polar graph for C6

Materials Research Proceedings 31 (2023) 227-239 https://doi.org/10.21741/9781644902592-24

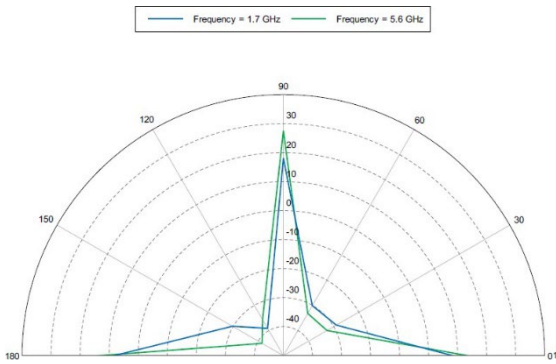

Fig 9. Polar graph for C7

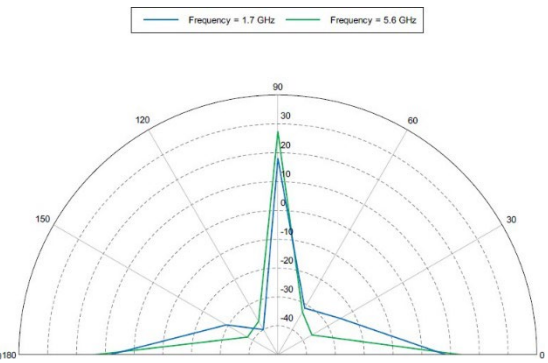

Fig 10. Polar graph for C8

As can be observed from the curves, at φ = 90˚, there is a sharp spike after the RCS being considerably low for φ = 30˚ and 60˚ and then declines sharply for 120˚ before increasing again at 150˚ and spiking at 180˚. This is the general trend for both high and low frequencies.

The notable configuration here is that of C2. While all other configurations result in RCS being between -50 dBsm and 30 dBsm, the RCS of C2 lies between 0 and -50 dBsm. The significance of RCS being below 0 dBsm is that RCS remains less than 1m2 in the entire frequency range. The RCS goes as low as -60 dBsm for φ = 150˚ at 5.6 Hz frequency. This is lower than all others where the minimum value is -40 dBsm.

Variable Chord at Root

Next, all other parameters constant were again kept constant and 8 models were created with varying values of chord length at the root. They were simulated and the RCS was compared with that of the original canard.

The parameters used are given below:

Table 2. Parameters of canards with variable chord at root

	Wing Span (one wing)	**Wing Chord (root)**	**Wing Chord (tip)**	**Aspect Ratio**
C9	3.81	2.0	0.6858	2.83
C10	3.81	1.8	0.6858	3.06
C11	3.81	1.5	0.6858	3.48
C12	3.81	1.2	0.6858	4.04
C13	3.81	2.4	0.6858	2.46
C14	3.81	2.7	0.6858	2.25
C15	3.81	3.0	0.6858	2.06
C16	3.81	3.3	0.6858	1.91

Materials Research Proceedings 31 (2023) 227-239 https://doi.org/10.21741/9781644902592-24

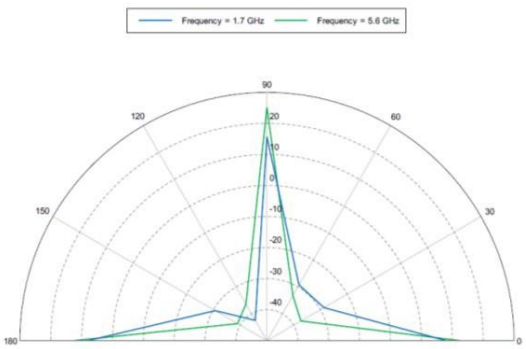

Fig 11. Polar graph for C9

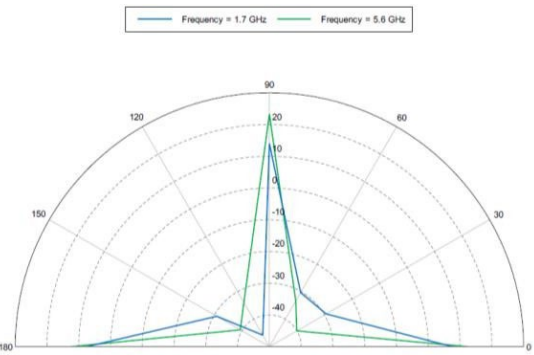

Fig 12. Polar graph for C10

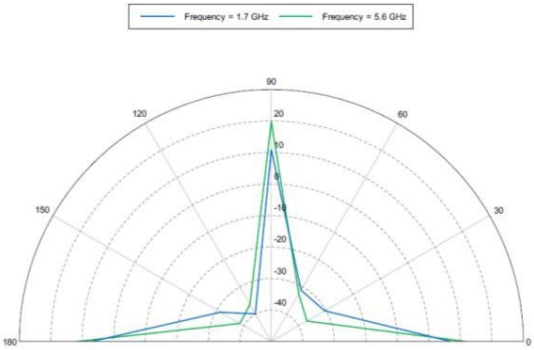

Fig 13. Polar graph for C11

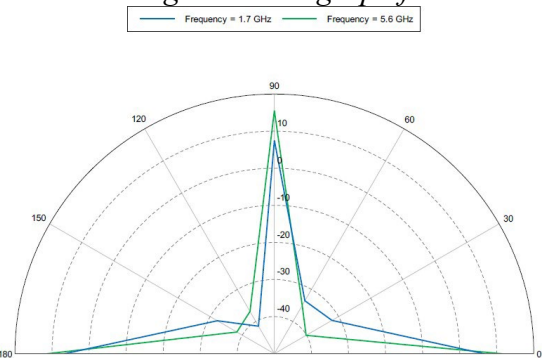

Fig 14. Polar graph for C12

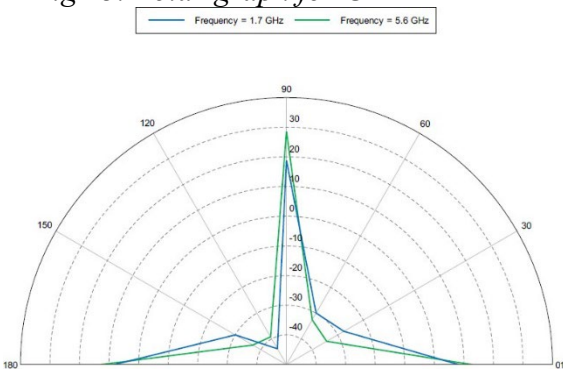

Fig 15. Polar graph for C13

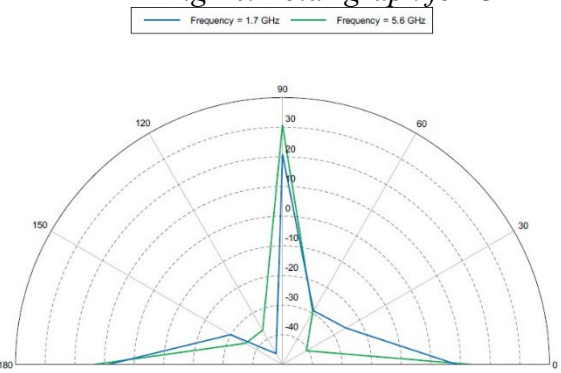

Fig 16. Polar graph for C14

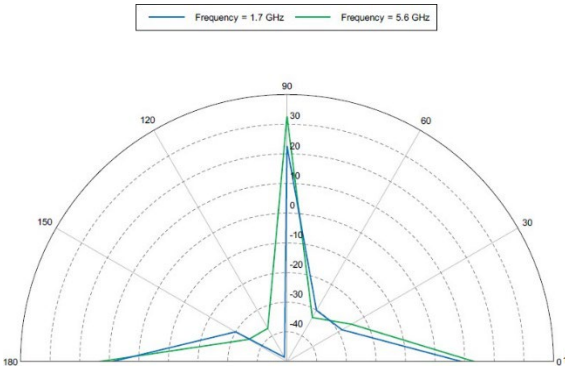

Fig 17. Polar graph for C15

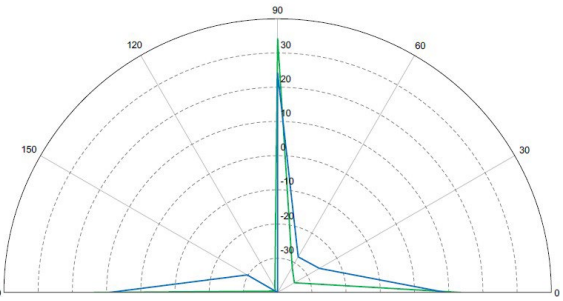

Fig 18. Polar graph for C16

Varying the chord at root sees a general trend between φ = 0˚ and 90˚. For 1.7 GHz frequency, the RCS increases and a spike occurs between 60˚ and 90˚. As the value of root chord increases, a sharper dip in RCS can be seen between φ = 90˚ and 120˚. It increases for 150˚ and spikes again for 180˚.

The high frequency curve follows irregular pattern for varying parameters. C16 configuration stands out for 5.6 GHz frequency RCS where a spike can be seen between 30˚ and 90˚ and an equally sharp dip from 90˚ to 150˚, spiking again at 180˚. The minimum value is -39.21 dBsm at 5.6 GHz and below -40 dBsm at 1.7 GHz.

Variable Wing Span

For the third case, the span was varied keeping all other parameters constant. The simulations results were compared with that obtained from the original parameters.

The span length used is specified below:

Table 3. Parameters of canard with variable span

	Wing Span (one wing)	**Wing Chord (root)**	**Wing Chord (tip)**	**Aspect Ratio**
C17	3.7	2.286	0.6858	2.49
C18	3.6	2.286	0.6858	2.42
C19	3.5	2.286	0.6858	2.35
C20	3.4	2.286	0.6858	2.28
C21	3.9	2.286	0.6858	2.62
C22	4.0	2.286	0.6858	2.69
C23	4.1	2.286	0.6858	2.75
C24	4.2	2.286	0.6858	2.82

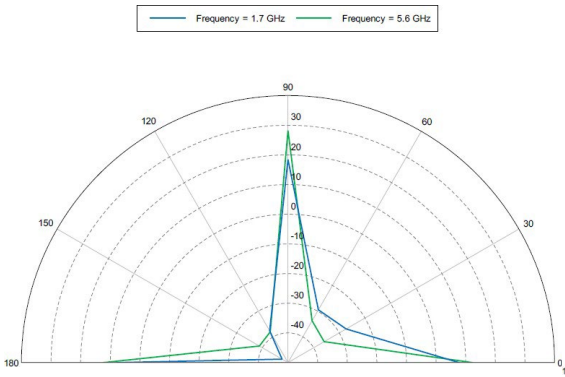

Fig 19. Polar graph for C17

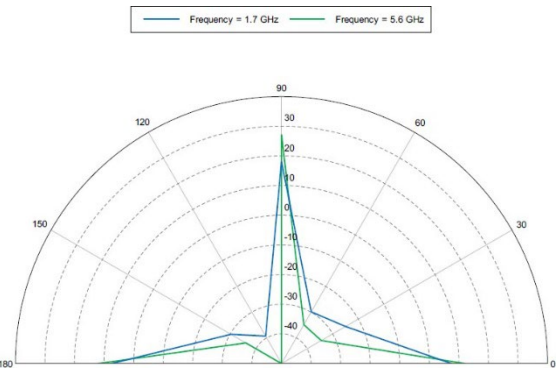

Fig 20. Polar graph for C18

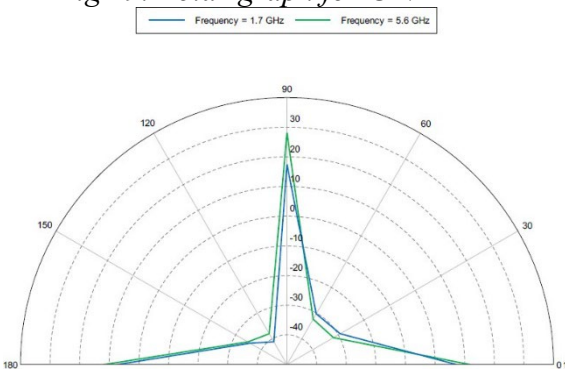

Fig 21. Polar graph for C19

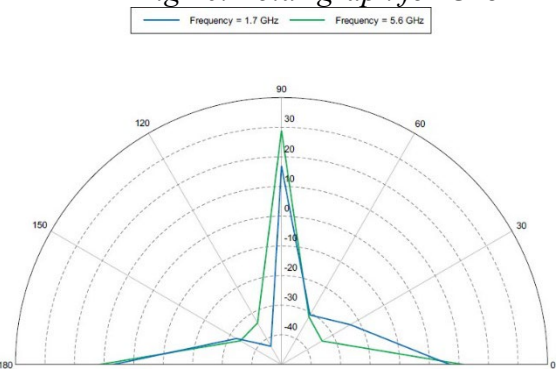

Fig 22. Polar graph for C20

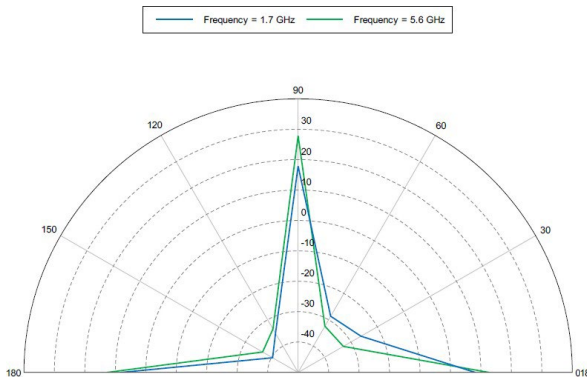

Fig 23. Polar graph for C21

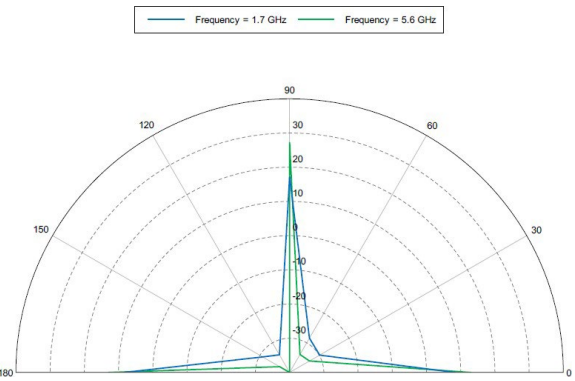

Fig 24. Polar graph for C22

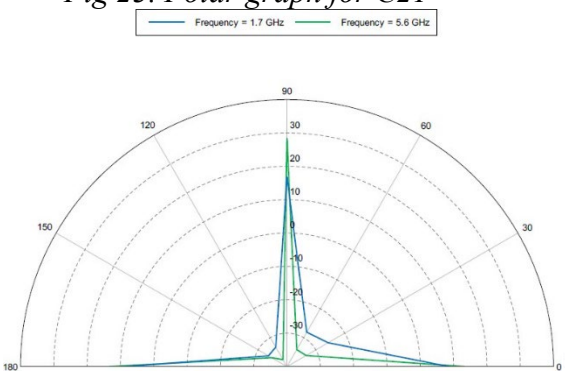

Fig 25. Polar graph for C23

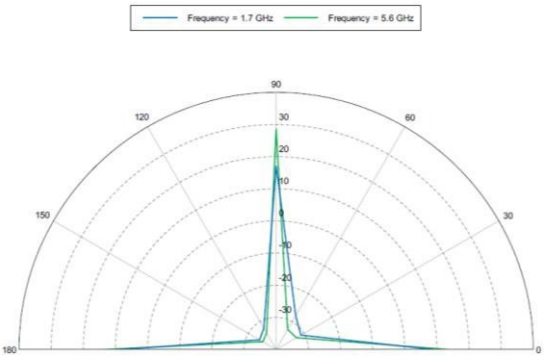

Fig 26. Polar graph for C24

For frequency 1.7 GHz, the longer canards see a steeper rise in RCS between 30˚ - 90˚ and similar sharp dip between 90˚ to 150˚. The dip reaches even lower values for longer canards in 5.6 GHz frequency. The canards having span lower than original one do not follow any trend as such. However, the RCS reaches as low as -50 dBsm for low frequency in C17 at 150˚ and high frequency in C18 at 120˚.

Conclusion

A general trend can be spotted irrespective of the constant and variable parameters for φ in the range 0˚-90˚ at 1.7GHz frequency (exceptions being C1, C3, C6, C8, C18 and C20). The RCS increases between 0˚- 30˚, then there is steeper rise between 30˚- 60˚ and then it spikes up to 90˚. Varying wing span does not affect the trend in general but longer wings see a direct and much steep rise between 30˚- 90˚. Variation in root chord of the wing gives different RCS trends, not following a specific pattern as such. Tip chord variation follows the same trend, the RCS increases between 0˚- 30˚, then there is steeper rise between 30˚- 60˚ and then it spikes up to 90˚ with the rise between 30˚- 90˚ being steeper and sharper than the others.

The C2 configuration stands out in all of the 24 models. The RCS for these parameters remains less than 1 m2 in the entire frequency range. The RCS is 1.37 × 10-7 m2 at φ = 150˚ for 5.6 GHz frequency and 8.71 × 10-7 m2 at φ = 120˚ for 1.7 GHz frequency, compared to the original parameters, where RCS reaches the minimum of 1.71 × 10- 5 m2 for high frequency.

Nomenclature

AR	Aspect ratio	--
θ	Angle between z axis and xy plane	(°)
φ	Roll angle	(°)

References

[1] "Stealth Technology". Wikipedia. 2022.

[2] S. M., Vaitheeswaran & Gowthami, T. "RCS of the Tail Swept Flying Wing and Comparison with Milestone Aircrafts". 2016.

[3] Michishita, Naobumi & Nguyen, Quoc Dinh & Yamada, Yoshihide. "Simulation and Measurement Methods for RCS Estimations of a Scale Model Airplane". REV Journal on Electronics and Communications. 5. 10.21553/rev-jec.93. 2016. https://doi.org/10.21553/rev-jec.93

[4] Ya-Qiang Zhuang, Chen-Xin Zhang & Xiao-Kuan Zhang. "Dynamic RCS Statistical Characterization of Aircraft Target Using Gaussian Mixture Density Model (GMDM)".

[5] Zhenghong, Gao, and Wang Mingliang. "An efficient algorithm for calculating aircraft RCS based on the geometrical characteristics." Chinese Journal of Aeronautics 21.4, 2008, pp. 296-303. https://doi.org/10.1016/S1000-9361(08)60039-4

[6] Van Schalkwyk, Richard F., and Johan C. Smit. "Dynamic radar cross section measurements of a full- scale aircraft for RCS modelling validation." 2017. https://doi.org/10.1049/cp.2017.0429

[7] Gou Zhanzhi, Chen Yingwen, MA Lianfeng. Radar cross-section effect of canard[J]. ACTA AERONAUTICAET ASTRONAUTICA SINICA, 2020, 41(6): 523485-523485.

[8] "Radar Cross Section (RCS)". Electronic Warfare and Radar Systems Engineering Handbook. https://www.rfcafe.com/references/electrical/ew- radar-handbook/radar-cross-section.htm

[9] Mahafza, B.R., "Radar Systems Analysis and Design using Matlab," CRC Press, 2000 Chapman &hall /crc, Boca Raton, London, New York, Washington, D.C. https://doi.org/10.1201/9781584888543

[10] "Basic Principles of The Method of Moments." Emagtech Wiki. 2018. http://www.emagtech.com/wiki/index.php/Basic_Principles_of_The_Method_of_Moments

[11] David L. Lynch Jr., "Introduction to stealth systems". An Introduction to RF Stealth (Radar, Sonar and Navigation), Institution of Engineering and Technology, 2021, pp. 42. https://doi.org/10.1049/SBRA540E

[12] Chibuisi, I. "Simulation of Radar Cross Section (RCS) of Spherical Objects". International Journal of Trend in Research and Development. Vol 2(5), 2015.

[13] "Basic Principles of Physical optics". Emagtech Wiki. 2018. http://www.emagtech.com/wiki/index.php/Basic_Principles_of_Physical_Optics

[14] Richardson, M. "Physical Optics Based Methods for Scattering Analysis". Thesis. Stellenbosch University. March 2018.

[15] Altair Engineering Inc, Altair FEKO 2021.1.2 User Guide. 2021.